



Phosphate and ammonium adsorption of sesame straw biochars produced at different pyrolysis temperatures

Qianqian Yin¹ · Bingdong Zhang¹ · Ruikun Wang¹ · Zhenghui Zhao¹

Received: 26 March 2017 / Accepted: 15 November 2017 / Published online: 27 November 2017
© Springer-Verlag GmbH Germany, part of Springer Nature 2017

Abstract

The adsorption of NH_4^+ and PO_4^{3-} by sesame straw biochars (C-300, C-500, and C-700) prepared under different temperatures (300, 500, and 700 °C) was investigated in this study. The physicochemical properties of the biochars were characterized using Brunauer–Emmett–Teller method, X-ray diffraction, scanning electron microscopy, and Fourier transform infrared spectrometry. In batch experiments, C-300 showed the best NH_4^+ adsorption capacity of 3.45 mg/g because of its abundant surface functional groups at low pyrolysis temperature. C-700 achieved the optimal PO_4^{3-} adsorption capacity of 34.17 mg/g because of its high Ca, Mg, and Al contents and high surface area at high pyrolysis temperature. The isothermal study showed that the Langmuir–Freundlich model could sufficiently describe the NH_4^+ and PO_4^{3-} adsorption values, indicating the multiple adsorption processes of nutrients on biochars. The maximum NH_4^+ adsorption capacity was 93.61 mg/g on C-300, whereas the maximum PO_4^{3-} adsorption capacity was as high as 116.58 mg/g on C-700. Kinetic study showed that NH_4^+ adsorption on C-300 was mainly controlled by intraparticle diffusion, and the pseudo-second-order model could well describe PO_4^{3-} adsorption on C-700.

Keywords Biochar · Phosphate · Ammonium · Adsorption · Pyrolysis temperature

Introduction

Water eutrophication, which has been a serious environmental problem for several decades, causes increasingly adverse ecosystem degradation (Ali and Aboul-Enein 2006; Ali et al. 2009; Boesch et al. 2001; Diaz and Rosenberg 2008; Smith 2003). Nitrogen (N) and phosphorus (P), as the two important nutrients that cause water eutrophication, mainly come from municipal, industrial, and agricultural activities (Paerl 2009). Biological processes, chemical precipitation, and physical method have been developed to remove excessive N and P from water bodies (Park et al. 2015; Zhang et al. 2011). However, the biological method is limited by its strict application conditions, and chemical precipitation method is hindered by its high chemical consumption and potential for secondary water pollution (Fang et al. 2014; Jung et al. 2015a;

Özacar 2003). Physical adsorption is advantageous over the other methods because of its economical and environmentally friendly features (Ali 2010, 2012, 2014; Ali et al. 2012; Ali and Gupta 2006; Ma et al. 2011). Recently, new adsorbents for the adsorption of various contaminants from water have been developed (Ali et al. 2016a, b, c, d, 2017). Therefore, discovering a low-cost and effective adsorbent for N and P adsorption from water is urgently needed (Khan et al. 2011).

Biochar, as the solid product of biomass thermochemical conversion under oxygen-limited conditions, has high carbon content and a porous structure (Demirbas and Arin 2010; Mašek et al. 2013). Biochar has recently received increased attention because of its great potential for environmental benefits. For example, biochar can be applied in soil to improve soil fertility and to reduce greenhouse gas emissions (Lehmann et al. 2006; Verheijen et al. 2009). Moreover, biochar can be utilized as an adsorbent to remove organic contaminants (pesticide, naphthalene, and *p*-nitrotoluene) or inorganic contaminants (Cu(II), Cd(II), and Cr(III)) from water (Chen et al. 2011; Pan et al. 2013; Wang et al. 2015a; Zheng et al. 2010). Furthermore, biochar is an efficient adsorbent for removing excess N and P from water. Yao et al. reported that biochar derived from anaerobically digested sugar beet tailings displays

Responsible editor: Guilherme L. Dotto

✉ Qianqian Yin
qqyin@ncepu.edu.cn

¹ Present address: Department of Power Engineering, North China Electric Power University, Yonghua North Street 619, Baoding 071003, People's Republic of China

a high PO_4^{3-} removal rate of approximately 73% (Yao et al. 2011a, b). La-modified biochar from oak sawdust significantly improves NH_4^+ and PO_4^{3-} adsorption by 1.9- and 4.5-fold compared with pristine biochar (Wang et al. 2015b). Therefore, biochar exhibits great potential as a cost-effective and highly efficient adsorbent. Moreover, the NH_4^+ -laden and PO_4^{3-} -laden biochars could be applied into soil as slow-release fertilizers.

The physicochemical characteristics of biochar are mainly dependent on the feedstock and pyrolysis conditions (Enders et al. 2012; Zhao et al. 2013). The properties of biochar also significantly affect adsorption performance. Vast amounts of agricultural residues are produced in China and are usually discarded as solid waste or burned off in stacks, causing loss of resources and environmental pollution (Ahmad et al. 2012). Thus, a treatment procedure for agricultural wastes by using them as feedstocks for biochar production should be proposed (Jung et al. 2015a). Pyrolysis temperature is an important factor in biochar production because the biochar properties, such as composition, porous structure, and surface property, vary greatly at different pyrolysis temperatures. Thus, the influence of pyrolysis temperature on the adsorption performance of biochar for NH_4^+ and PO_4^{3-} should be carried out, providing essential data for the large-scale practical application of biochar in the remediation of eutrophic water.

To our knowledge, the adsorption of N and P using biochar derived from agricultural residues has not been extensively studied. In this study, biochar was produced from sesame straw at different pyrolysis temperatures. The physicochemical properties of the produced biochar were characterized, and the biochar feasibility as NH_4^+ and PO_4^{3-} adsorbents was evaluated.

Materials and methods

Feedstock and biochar production

Raw sesame straw was locally collected for biochar production. The feedstock was washed and dried at 80 °C prior to pyrolysis. The prepared sesame straw was pyrolyzed in a tube furnace under N_2 atmosphere. For each experiment, the samples were heated to 300, 500, and 700 °C at a rate of 5 °C/min and maintained at the peak temperatures for 2 h. Biochar was collected after the furnace cooled down. Biochar yield was determined based on the weight of dried sesame straw for pyrolysis. The obtained biochar was ground and sieved into < 0.2 mm. The final biochars were designated as C-300, C-500, and C-700 based on the peak pyrolysis temperature.

Biochar characterization

N_2 adsorption–desorption isotherms were recorded at 77 K using a Micromeritics ASAP 2020 apparatus. Brunauer–

Emmett–Teller (BET) method was used to determine the specific surface area of biochar. Fourier transform infrared (FTIR) spectrometry (Bruker, Tensor 27) was used to obtain the spectra in the range of 600–4000 cm^{-1} . Powder X-ray diffraction (XRD) analysis was conducted on a PANalytical Empyrean X-ray diffractometer. Biochar morphology was characterized with a scanning electron microscopy (SEM) (JEOL, JSM-7001F). The chemical composition of biochar was performed using an Elemental Analyzer (Vario Macro Cube) and an X-ray fluorescence device (Ametek, Spectro iQ II).

Adsorption of NH_4^+ and PO_4^{3-}

To clarify the effects of pyrolysis temperature on NH_4^+ and PO_4^{3-} adsorption, batch experiments were conducted with each biochar. NH_4^+ and PO_4^{3-} stock solutions were prepared using NH_4Cl and KH_2PO_4 , respectively. For each run, 100 mg of the prepared biochar was mixed with 50 mL solutions at the concentration of 50 mg/L (NH_4^+ -N and PO_4^{3-} -P) and then shaken for 36 h at 120 rpm at 25 °C. Then, the supernatant was filtered using a membrane syringe filter to determine the concentrations of NH_4^+ and PO_4^{3-} . The NH_4^+ and PO_4^{3-} concentrations in the liquid phase were analyzed using Nessler's reagent colorimetric method and ammonium molybdate spectrophotometric method, respectively.

The adsorption kinetics was investigated. The adsorption conditions and initial concentrations of NH_4^+ -N and PO_4^{3-} -P were similar to those of the batch experiment. At appropriate time intervals, the mixtures were immediately filtered. Adsorption isotherms were also investigated similarly by mixing 100 mg biochar with 50 mL solutions at different concentrations of NH_4^+ -N and PO_4^{3-} -P (5–500 mg/L). The samples were collected and filtered to determine the corresponding equilibrium concentrations after 36 h.

The amounts of NH_4^+ and PO_4^{3-} adsorbed on the biochar were calculated using Eq. (1) as follows:

$$q_t = \frac{V}{m}(C_0 - C_t), \quad (1)$$

where q_t (mg/g) is the adsorbed amounts of NH_4^+ and PO_4^{3-} per unit weight of biochar at a given time; C_0 and C_t (mg/L) are the corresponding concentrations of NH_4^+ and PO_4^{3-} at the initial and given time, respectively; m (g) is the mass of the biochar; and V (L) is the solution volume.

Modeling the adsorption data

The adsorption properties of NH_4^+ and PO_4^{3-} on biochars derived from different pyrolysis temperatures were interpreted in two ways. First, the relationship between the adsorption capacity and adsorption time was described by the kinetic

models. Then, the maximum adsorption capacity of biochar was described by the isothermal models.

Adsorption kinetics

Adsorption kinetics of NH_4^+ and PO_4^{3-} were described by three typical kinetic models (Jung et al. 2015b). The pseudo-first-order and pseudo-second-order models are widely used to describe physisorption and chemisorption between the adsorbent and adsorbate, respectively. The intraparticle diffusion model was used to verify the rate-controlling step during adsorption, illustrated as follows:

$$\text{Pseudo-first-order} \quad q_t = q_e(1 - e^{-k_1 t}), \quad (2)$$

$$\text{Pseudo-second-order} \quad q_t = k_2 q_e^2 t / (1 + k_2 q_e t), \quad (3)$$

$$\text{Intraparticle diffusion} \quad q_t = k_3 t^{0.5} + C, \quad (4)$$

where q_e and q_t (mg/g) are the adsorption capacity of the adsorbent at the equilibrium time and at the given time, respectively; k_1 (h^{-1}), k_2 ($\text{g mg}^{-1} \text{h}^{-1}$), and k_3 ($\text{mg}^{-1} \text{h}^{-0.5}$) are the rate constants of the three kinetic models; and C is a constant.

Adsorption isotherm

Adsorption isotherms of NH_4^+ and PO_4^{3-} were analyzed by three typical isothermal models. The Langmuir model can describe the monolayer absorption of adsorbate on the adsorbent, and no interaction was observed between the adsorbate molecules (Sellaoui et al. 2017a, b). The Freundlich and Langmuir–Freundlich models are two empirical models usually used to describe the chemical adsorption of adsorbate on the heterogeneous surface (Jung and Ahn 2016).

$$\text{Langmuir} \quad q_e = k_l q_m C_e / (1 + k_l C_e), \quad (5)$$

$$\text{Freundlich} \quad q_e = k_f C_e^{1/n}, \quad (6)$$

$$\text{Langmuir-Freundlich} \quad q_e = k q_m C_e^{1/n} / (1 + k C_e^{1/n}), \quad (7)$$

where C_e (mg/L) is the equilibrium concentration; k_l (L/mg), k_f ($\text{mg}^{1-1/n} \text{L}^{1/n} \text{g}^{-1}$), and k ($\text{L}^{1/n} / \text{mg}^{1/n}$) are the constants; q_m (mg/g) denotes the maximum adsorption capacity; and $1/n$ is the heterogeneity factor.

Results and discussion

Biochar characterization

Biochar yield and composition

The biochar yields for C-300, C-500, and C-700 were 35.21, 26.13, and 19.44% (Table 1), respectively, which decreased

with peak pyrolysis temperature. During biomass pyrolysis, the long-chain lignocellulosic components of biomass decomposed into short-chain components in the form of liquid bio-oil or gaseous biogas; the remaining components were the solid product biochar (Al-Wabel et al. 2013). Therefore, less biochar was recovered at high pyrolysis temperature because of the enhanced degradation of lignocellulosic structures. In addition, the carbonization degree of biochar was greatly promoted by increasing the temperature, indicating that the obtained biochar will be stable and beneficial for carbon sequestration.

The elemental compositions of biomass and biochars are listed in Table 1, which shows that C content significantly increased as temperature increased, whereas H and O contents showed the inverse tendency. This finding was consistent with the results of biochar yield because at high temperatures, numerous chemical bonds (C–H and C–O) are cleaved, thereby increasing the loss of H and O in the forms of CH_4 , H_2O , CO , and CO_2 (Ahmad et al. 2012; Chattopadhyaya et al. 2006). The calculated O/C and H/C ratios decreased as temperature increased, which also signified that less original organic components (such as polymeric CH_2 , fatty acid, lignin, and some cellulose) were preserved at high temperatures (Chen et al. 2011). Moreover, the decreased (O+N)/C ratio implied that the polar functional groups in biochar decreased as temperature increased (Ahmad et al. 2012). Some metallic elements (Ca, Mg, and Al) from the raw biomass accumulated in biochar samples. The contents of these elements also increased with pyrolysis temperature. These properties enhance the potential of biochar as a material with valuable applications.

Textural properties of biochar

The textural properties of the biochars were characterized by N_2 adsorption–desorption analysis and are summarized in Table 2. The BET surface areas of the biochars significantly increased with increasing pyrolysis temperature, especially from 500 to 700 °C. The porous structure of biochar became highly developed at high temperatures because volatiles were rapidly released from the biomass structure, resulting in pore formation. C-300 possessed the smallest surface area, whereas the surface area of C-700 was as high as $413 \text{ m}^2/\text{g}$ because numerous pores were generated via volatilization. The developed pore structure and large surface area play an important role in the adsorptive properties of biochar by providing a large available space for contaminant adsorption.

The morphologies of the biochars were analyzed using SEM. The SEM images are presented in Fig. 1. C-300 and C-500 showed relatively smooth surfaces. This result was consistent with the findings from the N_2 adsorption–desorption that these two biochars displayed underdeveloped pore structures and mainly retained the intrinsic nature of the

Table 1 Elemental composition of the biochars

Sample	Yield (%)	C (%)	H (%)	O (%)	N (%)	O/C ^a	H/C ^a	(O+N)/C ^a	Ca (%)	Mg (%)	Al (%)
Sesame straw	–	50.46	5.56	41.24	0.58	0.82	0.11	0.83	–	–	–
C-300	35.21	72.94	4.08	16.69	1.43	0.23	0.06	0.25	1.19	0.23	0.02
C-500	26.13	81.09	1.76	3.26	1.14	0.04	0.02	0.05	3.07	0.58	0.04
C-700	19.44	81.79	0.99	1.84	1.32	0.02	0.01	0.04	3.70	0.75	0.05

– not determined

^a Estimated on the mass/mass basis

feedstock biomass. However, C-700 showed a rough and porous structure with a high BET surface area.

As shown in Fig. 2, the crystal structure of each biochar was analyzed using XRD. All the XRD patterns of the biochar showed two broad diffraction peaks at 20–30° and 40–50°. These peaks could be ascribed to the reflections of graphite. In addition, the peak at 40–50° narrowed with the increase of carbonization temperature, indicating that high temperatures are beneficial for the formation of a graphite-like structure (Yu et al. 2010). Some diffraction peaks assigned to Ca and Mg compounds were also detected in the XRD patterns of C-500 and C-700.

The FTIR spectra of the different biochars are shown in Fig. 3a. The spectra revealed that the amount of functional groups in the biochars gradually decreased with increasing pyrolysis temperature. The visible peaks at approximately 3407, 2923, 1630, 1578, 1422, and 1055 cm⁻¹ indicated that considerable amounts of original organic residues were preserved in C-300, whereas most of these compounds disappeared from C-700. This phenomenon was in line with the results of the referred work that carbonization was enhanced at high carbonization temperatures with the loss of oxygen-containing species (Ahmad et al. 2012; Chen et al. 2008). Some visible peaks located at 1000–600 cm⁻¹ could be assigned to the metal–oxygen bonds (Chandradass and Kim 2010).

NH₄⁺ and PO₄³⁻ adsorption

Batch experiment

Batch experiments were carried out to evaluate the NH₄⁺ and PO₄³⁻ adsorption capacities of the biochars produced at different pyrolysis temperatures. As shown in Fig. 4, C-300, C-500,

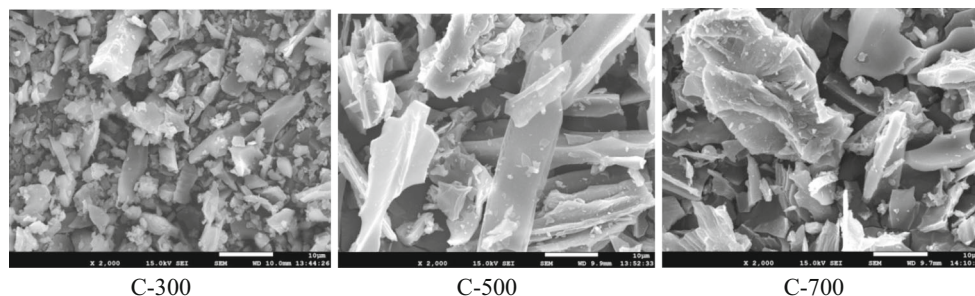
and C-700 achieved NH₄⁺ adsorption values of 3.45, 0.91, and 1.62 mg/g, respectively. The highest NH₄⁺ adsorption was achieved by C-300, as derived from the lowest temperature. This result was consistent with that of the referred work, wherein good NH₄⁺ adsorption was achieved by the biochar generated from low pyrolysis temperature (Gao et al. 2015). The physicochemical properties of biochar, especially porosity and surface functional groups, play important roles in NH₄⁺ adsorption (Kizito et al. 2015; Liu et al. 2010). However, the NH₄⁺ adsorption capacity of C-700, which had the highest surface area, was lower than that of C-300, which had the lowest surface area. This result suggested that the large surface area is not the main contributor to NH₄⁺ removal. As previously reported, the polar functional groups, such as hydroxyl, phenol, and carboxyl groups, are the main active groups that participate in NH₄⁺ adsorption (Liu et al. 2010). Interestingly, FTIR analysis revealed that C-300 was rich in functional groups. To determine the functional groups involved in the NH₄⁺ adsorption, the FTIR spectra of C-300 before and after NH₄⁺ adsorption were analyzed and presented in Fig. 3b. The wave numbers shifted from 1422 and 1578 cm⁻¹ to 1440 and 1602 cm⁻¹ after NH₄⁺ adsorption, respectively, confirming that the alkyl and carboxylic groups might be involved in adsorption (Wahab et al. 2010). Therefore, NH₄⁺ adsorption by sesame straw biochar was dominated by the surface functional groups, and a low pyrolysis temperature was beneficial for the preservation of the surface functional groups.

The biochars exhibited remarkably different PO₄³⁻ removal capabilities (Fig. 5). For C-300, the negative value of PO₄³⁻ adsorption representing the residual PO₄³⁻ concentration after 36-h batch adsorption was higher than the initial concentration, indicating that PO₄³⁻ was released from C-300 into the

Table 2 Textural properties of the biochars

Sample	S _{BET} (m ² /g)	S _{micro} (m ² /g)	S _{external} (m ² /g)	V _{pore} (cm ³ /g)	V _{micro} (cm ³ /g)	V _{external} (cm ³ /g)	D _{pore} (nm)
C-300	2.92	0.81	2.11	0.0085	0.0003	0.0082	11.61
C-500	19.16	12.44	6.72	0.0119	0.0048	0.0071	2.48
C-700	413.46	302.60	110.86	0.2074	0.1218	0.0856	2.01

Fig. 1 SEM images of different biochars



solution. This result was consistent with the referred work that PO_4^{3-} would be released from the cacao shell and corn cob biochars (Hale et al. 2013). Therefore, it could be interpreted that the amount of the adsorbed PO_4^{3-} was less than the released PO_4^{3-} of C-300. The biochar surfaces are usually negatively charged, providing difficulty for adsorption of negatively charged ions, such as PO_4^{3-} (Eberhardt et al. 2006; Krishnan and Haridas 2008). Thus, the poor adsorption capacity of C-300 likely resulted from electrostatic repulsion between PO_4^{3-} and the biochar (Ren et al. 2015). By contrast, C-500 and C-700 showed positive PO_4^{3-} adsorption. C-700, in particular, adsorbed 34.17 mg- PO_4^{3-} /g, which was considerably higher than that adsorbed by the La-modified biochar (19.75 mg- PO_4^{3-} /g) (Wang et al. 2015b). Metal oxides play an important role in the adsorption of negatively charged ions by the formation of mono-, bi-, and tri-nuclear complexes on the biochar (Yao et al. 2011b, 2013; Zhang et al. 2012). In this study, the adsorption capacity of PO_4^{3-} was positively correlated with the metallic element content of biochar (Table 1). Previous studies also reported that the biochar produced from digested sugar beet tailings exhibits excellent PO_4^{3-} adsorption because of the presence of Mg and Ca (Yao et al. 2011a, b). Therefore, the enhanced Ca, Mg, and Al contents of biochar with increased temperature likely enhance PO_4^{3-} adsorption

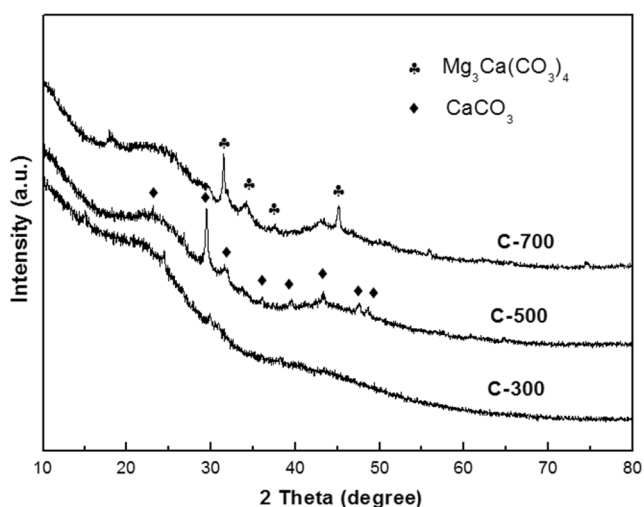


Fig. 2 XRD patterns of different biochars

capacity. In addition, the high surface area and pore volume could provide sufficient space and binding sites, greatly contributing to the high PO_4^{3-} adsorption capacity of biochar derived from high temperature. Therefore, all these results indicated that C-700 derived from sesame straw displays great potential as an effective PO_4^{3-} adsorbent.

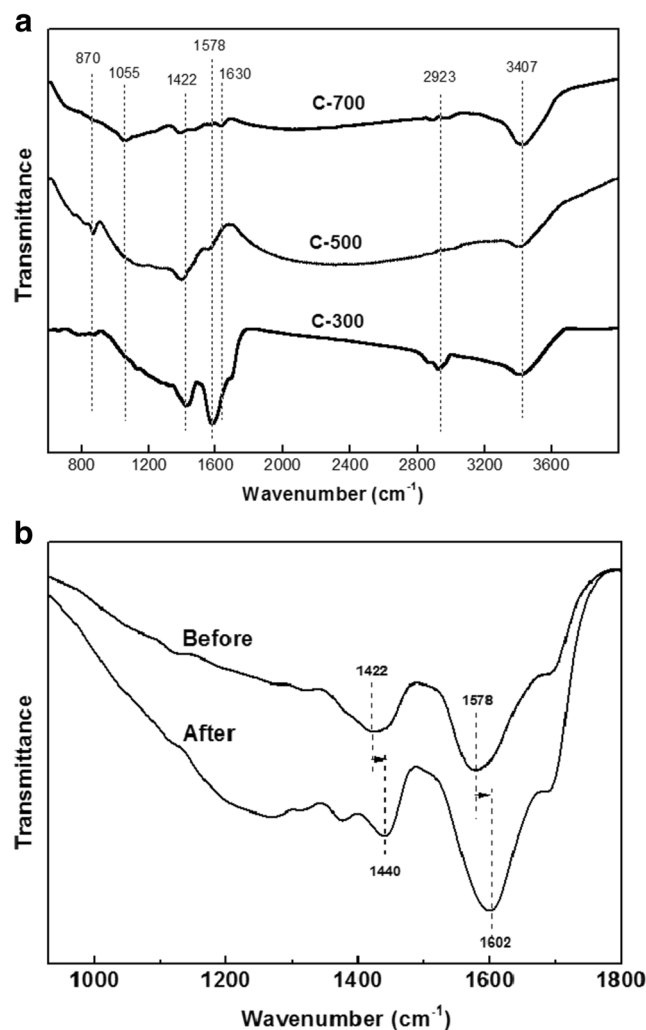


Fig. 3 a FTIR spectra of different biochars. b Magnified FTIR spectra (900–1800 cm^{-1}) of C-300 before and after NH_4^+ adsorption (“After” denoted the C-300 after 36-h adsorption of NH_4^+ with the initial NH_4^+ –N concentration of 50 mg/L)

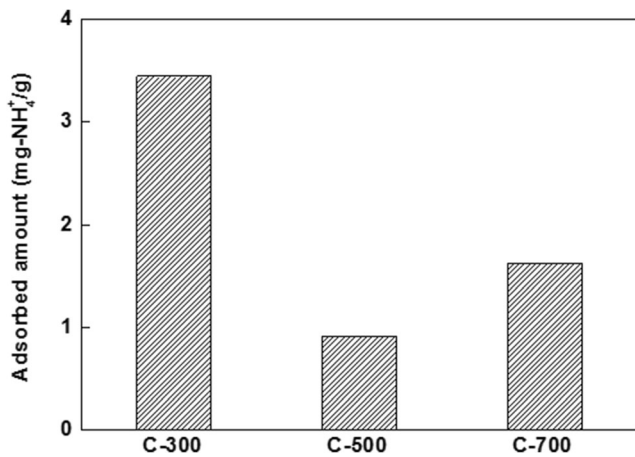


Fig. 4 NH₄⁺ adsorption of different biochars (Initial concentration of N H₄⁺ -N was 50 mg/L, and adsorption duration was maintained at 36 h)

Adsorption kinetics and isotherms of NH₄⁺

Kinetic studies were conducted to determine the adsorption time that is required to achieve the adsorption equilibrium. The adsorption kinetics curves of different biochars for NH₄⁺ adsorption are plotted in Fig. 6a, and the best-fit parameters of each model are listed in Table 3. The kinetic curves of C-500 and C-700 for NH₄⁺ adsorption could reach the equilibrium in approximately 20 and 6 h, respectively. The pseudo-second-order model could well describe the NH₄⁺ adsorption of C-500 and C-700, with the correlation coefficients (*R*²) of 0.966 and 0.958, respectively. Moreover, the calculated *q_e* values from the pseudo-second-order model were in close range with the experimental values, which further confirmed that the pseudo-second-order model had the best-fit. It is suggested that the NH₄⁺ adsorption of C-500 and C-700 was mainly controlled by chemisorption (Ho 2006). However, the NH₄⁺ adsorption of C-300 was well explained in terms of the intraparticle diffusion model with the high regression

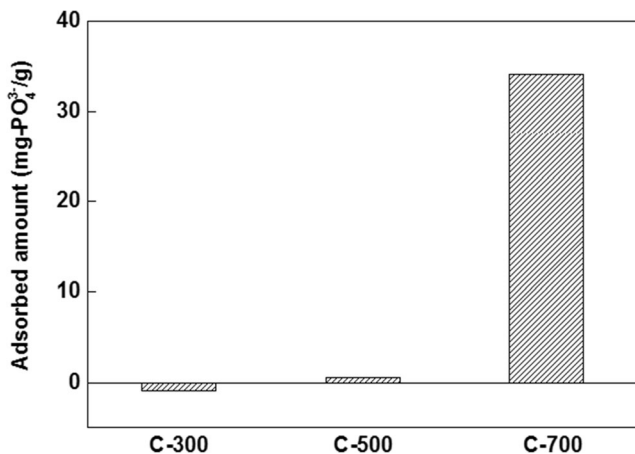


Fig. 5 PO₄³⁻ adsorption of different biochars (Initial concentration of PO₄³⁻ -P was 50 mg/L, and adsorption duration was maintained at 36 h)

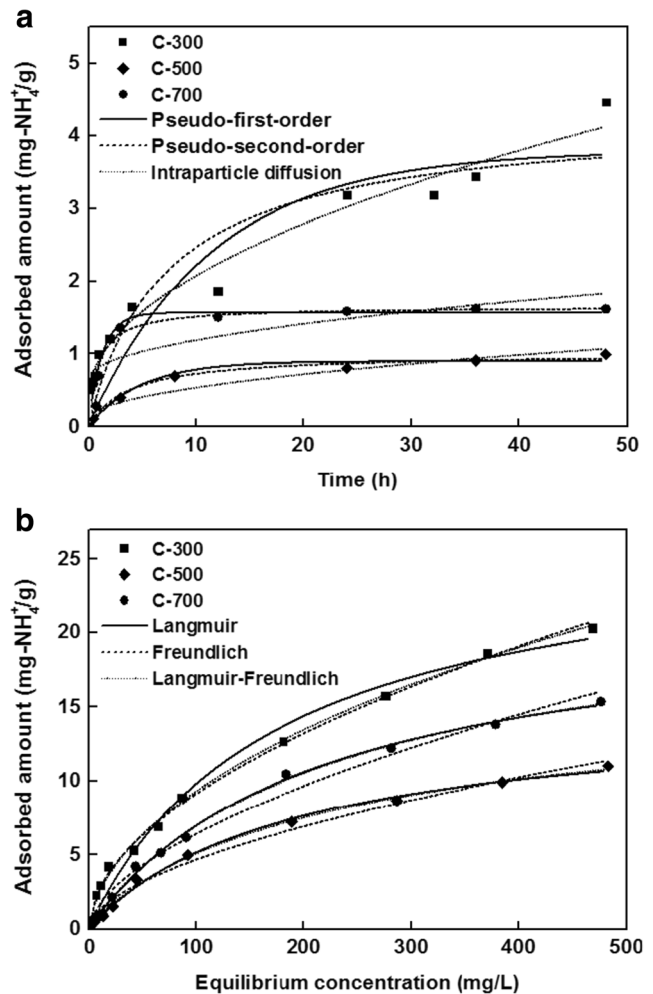


Fig. 6 Adsorption a kinetics and b isotherms of NH₄⁺ on different biochars

coefficient (*R*² = 0.970) and the small value of intercept (*C* = 0.365). Intraparticle surface diffusion was considered the major mechanism for NH₄⁺ adsorption of C-300. This result was consistent with the conclusion of previous studies that intraparticle surface diffusion mainly controlled the sorption of contaminants by biochar (Kizito et al. 2015; Yao et al. 2011b).

The NH₄⁺ adsorption data of each biochar were fitted to three adsorption isothermal models. The results are shown in Fig. 6b, and the corresponding parameters are listed in Table 4. The Langmuir–Freundlich model precisely agreed with the NH₄⁺ adsorption of C-300, C-500, and C-700 with high *R*² (> 0.995). The calculated maximum capacities of NH₄⁺ adsorption of C-300, C-500, and C-700 were 93.61, 16.95, and 23.07 mg/g, respectively, which were higher than those of many other NH₄⁺ adsorbents (Jellali et al. 2011; Sarkhot et al. 2013; Zhang et al. 2014). This finding indicated that NH₄⁺ adsorption by sesame biochar was controlled by chemisorption and

Table 3 Parameters of NH_4^+ and PO_4^{3-} adsorption kinetics

Sample	Adsorbate	Pseudo-first-order			Pseudo-second-order			Intraparticle diffusion		
		k_1	q_e	R^2	k_2	q_e	R^2	k_3	C	R^2
C-300	NH_4^+	0.088	3.79	0.809	0.032	4.26	0.858	0.542	0.365	0.970
C-500	NH_4^+	0.209	0.90	0.946	0.261	1.01	0.966	0.140	0.953	0.893
C-700	NH_4^+	0.768	1.57	0.933	0.678	1.65	0.958	0.170	0.649	0.730
C-700	PO_4^{3-}	1.238	31.88	0.820	0.052	33.60	0.928	3.198	15.925	0.854

multiple processes (Fang et al. 2014; Yao et al. 2011b). The value of $1/n$ is an indicator of the heterogeneity of biochar surface (Tseng and Wu 2008). The interaction between the biochar and NH_4^+ will become strong when the value of $1/n$ becomes small. In this study, the value of $1/n$ increased with temperature. Therefore, the biochar derived from low temperature was favorable for NH_4^+ adsorption, which was consistent with the highest NH_4^+ adsorption capacity of C-300.

Adsorption kinetics and isotherms of PO_4^{3-}

The adsorption kinetics and adsorption isotherms of C-700 were investigated because of its excellent PO_4^{3-} adsorption capacity, and the adsorption data were fitted to typical kinetic models (Fig. 7a) and isothermal models (Fig. 7b). C-700 exhibited a strong PO_4^{3-} adsorption in the entire time range and could reach the adsorption equilibrium in approximately 12 h. The pseudo-second-order model showed the best-fit for PO_4^{3-} adsorption on C-700, and the calculated q_e value (Table 3) based on the pseudo-second-order model was close to the experimental result. This finding indicated that PO_4^{3-} adsorption on C-700 was mainly controlled by chemical actions (Fang et al. 2015; Radnia et al. 2011). The intraparticle diffusion model did not pass through the origin ($C=15.925$), indicating that the PO_4^{3-} adsorption of C-700 was controlled by external and internal diffusion (Jung et al. 2015b).

For the isothermal investigation, the Freundlich and Langmuir–Freundlich models well described PO_4^{3-} adsorption, considering that the R^2 values of these two models were the same. The PO_4^{3-} adsorption capacity of C-700 was controlled by multiple processes, consistent with that in the referred work (Fang et al. 2015; Yao et al. 2013). The maximum PO_4^{3-} adsorption capacity of C-700 reached as high as 116.58 mg/g (Table 4), indicating that the biochar could be used as an efficient sorbent to remove PO_4^{3-} from water. In addition, this high adsorption capacity suggested that the post-adsorbed biochar could potentially be used as a P-fertilizer (Yao et al. 2013).

Conclusions

Pyrolysis temperature exhibits great effect on biochar properties, further influencing the adsorption properties of biochar. Sesame straw biochars were produced at 300, 500, and 700 °C, and their adsorption capacities for NH_4^+ and PO_4^{3-} were investigated in this work. C-300 and C-700 showed the best NH_4^+ and PO_4^{3-} adsorption, respectively, with the maximum adsorption capacity of 93.61 mg- NH_4^+ /g and 116.58 mg- PO_4^{3-} /g accordingly. The abundant functional groups of C-300 were the main contributors to the high NH_4^+ adsorption. The large surface area and high Ca, Mg, and Al contents were responsible for the high PO_4^{3-} adsorption of

Table 4 Parameters of NH_4^+ and PO_4^{3-} adsorption isotherms

Sample	Adsorbate	Langmuir			Freundlich			Langmuir–Freundlich			
		k_1	q_m	R^2	k_f	n	R^2	k	n	q_m	R^2
C-300	NH_4^+	0.006	26.84	0.983	0.797	1.887	0.995	0.007	1.661	93.61	0.996
C-500	NH_4^+	0.005	14.81	0.997	0.345	1.767	0.988	0.007	1.116	16.95	0.997
C-700	NH_4^+	0.005	21.90	0.997	0.434	1.707	0.987	0.005	1.043	23.07	0.997
C-700	PO_4^{3-}	2.994	45.27	0.778	21.390	6.558	0.940	0.226	4.645	116.58	0.940

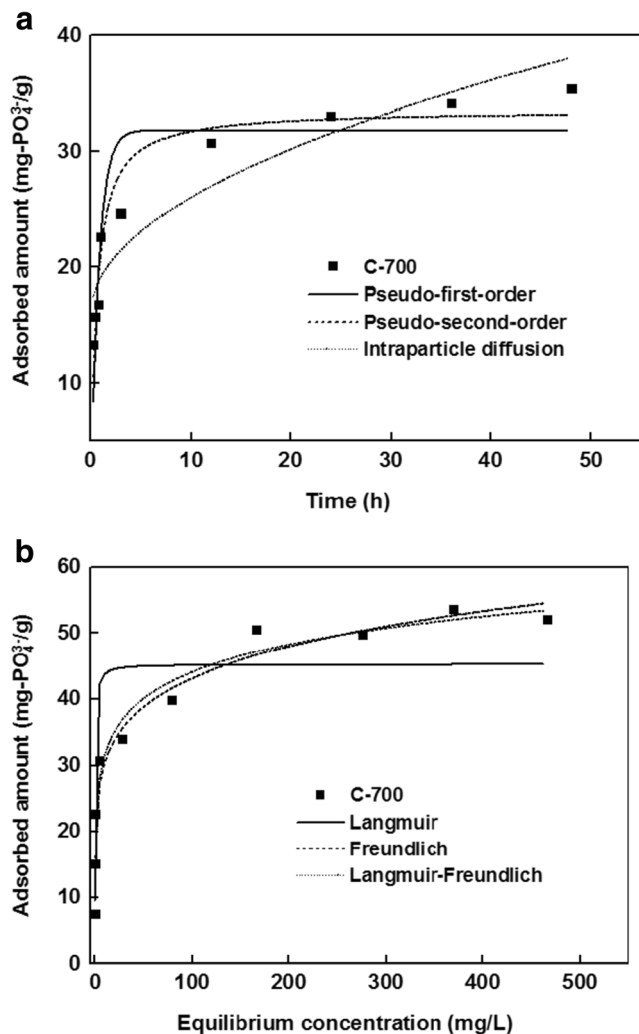


Fig. 7 Adsorption **a** kinetics and **b** isotherms of PO_4^{3-} on C-700

C-700. Thus, sesame straw biochar has enormous potential to be used in eutrophic water remediation to adsorb NH_4^+ and PO_4^{3-} . Moreover, the biochar loaded with N or P nutrients could be used as a slow-release fertilizer to improve the soil fertility. Thus, a feasible method to deal with the large amount of agricultural residues and water eutrophication is achieved.

Acknowledgements This work was supported by the National Natural Science Foundation of China (No. 51506054), the Natural Science Foundation of Hebei Province (No. E2016502089), and the Fundamental Research Funds for the Central Universities (No. 2015MS118).

References

Ahmad M, Lee SS, Dou X, Mohan D, Sung J-K, Yang JE, Ok YS (2012) Effects of pyrolysis temperature on soybean stover- and peanut shell-derived biochar properties and TCE adsorption in water.

Bioresour Technol 118:536–544. <https://doi.org/10.1016/j.biortech.2012.05.042>

Al-Wabel MI, Al-Omran A, El-Naggar AH, Nadeem M, Usman ARA (2013) Pyrolysis temperature induced changes in characteristics and chemical composition of biochar produced from conocarpus wastes. *Bioresour Technol* 131:374–379. <https://doi.org/10.1016/j.biortech.2012.12.165>

Ali I (2010) The quest for active carbon adsorbent substitutes: inexpensive adsorbents for toxic metal ions removal from wastewater. *Sep Purif Rev* 39(3-4):95–171. <https://doi.org/10.1080/15422119.2010.527802>

Ali I (2012) New generation adsorbents for water treatment. *Chem Rev* 112(10):5073–5091. <https://doi.org/10.1021/cr300133d>

Ali I (2014) Water treatment by adsorption columns: evaluation at ground level. *Sep Purif Rev* 43(3):175–205. <https://doi.org/10.1080/15422119.2012.748671>

Ali I, Aboul-Enein HY (2006) Instrumental methods in metal ions speciation: chromatography, capillary electrophoresis and electrochemistry. Taylor & Francis Ltd., USA. <https://doi.org/10.1201/9781420019407>

Ali I, Aboul-Enein HY, Gupta VK (2009) Nano chromatography and capillary electrophoresis: pharmaceutical and environmental analyses. Wiley & Sons, USA

Ali I, Al-Othman ZA, Alharbi OML (2016a) Uptake of pantoprazole drug residue from water using novel synthesized composite iron nano adsorbent. *J Mol Liq* 218:465–472. <https://doi.org/10.1016/j.molliq.2016.02.088>

Ali I, Al-Othman ZA, Alwarthan A (2016b) Green synthesis of functionalized iron nano particles and molecular liquid phase adsorption of ametryn from water. *J Mol Liq* 221:1168–1174. <https://doi.org/10.1016/j.molliq.2016.06.089>

Ali I, Al-Othman ZA, Alwarthan A (2016c) Molecular uptake of congo red dye from water on iron composite nano particles. *J Mol Liq* 224:171–176. <https://doi.org/10.1016/j.molliq.2016.09.108>

Ali I, Al-Othman ZA, Alwarthan A (2016d) Synthesis of composite iron nano adsorbent and removal of ibuprofen drug residue from water. *J Mol Liq* 219:858–864. <https://doi.org/10.1016/j.molliq.2016.04.031>

Ali I, Al-Othman ZA, Alwarthan A (2017) Uptake of propranolol on ionic liquid iron nanocomposite adsorbent: kinetic, thermodynamics and mechanism of adsorption. *J Mol Liq* 236:205–213. <https://doi.org/10.1016/j.molliq.2017.04.028>

Ali I, Asim M, Khan TA (2012) Low cost adsorbents for the removal of organic pollutants from wastewater. *J Environ Manag* 113:170–183. <https://doi.org/10.1016/j.jenvman.2012.08.028>

Ali I, Gupta VK (2006) Advances in water treatment by adsorption technology. *Nat Protoc* 1(6):2661–2667. <https://doi.org/10.1038/nprot.2006.370>

Boesch D, Burreson E, Dennison W, Houde E, Kemp M, Kennedy V, Newell R, Paynter K, Orth R, Ulanowicz R (2001) Factors in the decline of coastal ecosystems. *Science* 293(5535):1589–1591

Chandradass J, Kim KH (2010) Effect of precursor ratios on the synthesis of $MgAl_2O_4$ nanoparticles by a reverse microemulsion method. *J Ceram Process Res* 11:96–99

Chattopadhyaya G, Macdonald DG, Bakhshi NN, Soltan Mohammadzadeh JS, Dalai AK (2006) Preparation and characterization of chars and activated carbons from Saskatchewan lignite. *Fuel Process Technol* 87(11):997–1006. <https://doi.org/10.1016/j.fuproc.2006.07.004>

Chen B, Zhou D, Zhu L (2008) Transitional adsorption and partition of nonpolar and polar aromatic contaminants by biochars of pine needles with different pyrolytic temperatures. *Environ Sci Technol* 42(14):5137–5143. <https://doi.org/10.1021/es8002684>

Chen BL, Chen ZM, Lv SF (2011) A novel magnetic biochar efficiently sorbs organic pollutants and phosphate. *Bioresour Technol* 102(2):716–723. <https://doi.org/10.1016/j.biortech.2010.08.067>

- Demirbas A, Arin G (2010) An overview of biomass pyrolysis. *Energy Sources* 24:471–482
- Diaz RJ, Rosenberg R (2008) Spreading dead zones and consequences for marine ecosystems. *Science* 321(5891):926–929. <https://doi.org/10.1126/science.1156401>
- Eberhardt TL, Min SH, Han JS (2006) Phosphate removal by refined aspen wood fiber treated with carboxymethyl cellulose and ferrous chloride. *Bioresour Technol* 97(18):2371–2376. <https://doi.org/10.1016/j.biortech.2005.10.040>
- Enders A, Hanley K, Whitman T, Joseph S, Lehmann J (2012) Characterization of biochars to evaluate recalcitrance and agronomic performance. *Bioresour Technol* 114:644–653. <https://doi.org/10.1016/j.biortech.2012.03.022>
- Fang C, Zhang T, Li P, Jiang R, Wu S, Nie H, Wang Y (2015) Phosphorus recovery from biogas fermentation liquid by Ca-Mg loaded biochar. *J Environ Sci* 29:106–114. <https://doi.org/10.1016/j.jes.2014.08.019>
- Fang C, Zhang T, Li P, Jiang RF, Wang YC (2014) Application of magnesium modified corn biochar for phosphorus removal and recovery from swine wastewater. *Int J Environ Res Public Health* 11(9):9217–9237. <https://doi.org/10.3390/ijerph110909217>
- Gao F, Xue YW, Deng PY, Cheng XR, Yang K (2015) Removal of aqueous ammonium by biochars derived from agricultural residuals at different pyrolysis temperatures. *Chem Speciat Bioavailab* 27(2):92–97. <https://doi.org/10.1080/09542299.2015.1087162>
- Hale SE, Alling V, Martinsen V, Mulder J, Breedveld GD, Cornelissen G (2013) The sorption and desorption of phosphate-P, ammonium-N and nitrate-N in cacao shell and corn cob biochars. *Chemosphere* 91(11):1612–1619. <https://doi.org/10.1016/j.chemosphere.2012.12.057>
- Ho Y-S (2006) Review of second-order models for adsorption systems. *J Hazard Mater* 136(3):681–689. <https://doi.org/10.1016/j.jhazmat.2005.12.043>
- Jellali S, Wahab MA, Anane M, Riahi K, Jedidi N (2011) Biosorption characteristics of ammonium from aqueous solutions onto *Posidonia oceanica* (L.) fibers. *Desalination* 270(1-3):40–49. <https://doi.org/10.1016/j.desal.2010.11.018>
- Jung KW, Ahn KH (2016) Fabrication of porosity-enhanced MgO/biochar for removal of phosphate from aqueous solution: application of a novel combined electrochemical modification method. *Bioresour Technol* 200:1029–1032. <https://doi.org/10.1016/j.biortech.2015.10.008>
- Jung KW, Hwang MJ, Ahn KH, Ok YS (2015a) Kinetic study on phosphate removal from aqueous solution by biochar derived from peanut shell as renewable adsorptive media. *Int J Environ Sci Technol* 12(10):3363–3372. <https://doi.org/10.1007/s13762-015-0766-5>
- Jung KW, Jeong TU, Hwang MJ, Kim K, Ahn KH (2015b) Phosphate adsorption ability of biochar/Mg-Al assembled nanocomposites prepared by aluminum-electrode based electro-assisted modification method with MgCl₂ as electrolyte. *Bioresour Technol* 198:603–610. <https://doi.org/10.1016/j.biortech.2015.09.068>
- Khan TA, Sharma S, Ali I (2011) Adsorption of Rhodamine B dye from aqueous solution onto acid activated mango (*Mangifera indica*) leaf powder: equilibrium, kinetic and thermodynamic studies. *J Toxicol Environ Heal Sci* 3:286–297
- Kizito S, Wu S, Kipkemoi KW, Lei M, Lu Q, Bah H, Dong R (2015) Evaluation of slow pyrolyzed wood and rice husks biochar for adsorption of ammonium nitrogen from piggery manure anaerobic digestate slurry. *Sci Total Environ* 505:102–112. <https://doi.org/10.1016/j.scitotenv.2014.09.096>
- Krishnan KA, Haridas A (2008) Removal of phosphate from aqueous solutions and sewage using natural and surface modified coir pith. *J Hazard Mater* 152(2):527–535. <https://doi.org/10.1016/j.jhazmat.2007.07.015>
- Lehmann J, Gaunt J, Rondon M (2006) Bio-char sequestration in terrestrial ecosystems—a review. *Mitig Adapt Strateg Glob Chang* 11:395–419
- Liu H, Dong Y, Wang H, Yun L (2010) Ammonium adsorption from aqueous solutions by strawberry leaf powder: equilibrium, kinetics and effects of coexisting ions. *Desalination* 263(1-3):70–75. <https://doi.org/10.1016/j.desal.2010.06.040>
- Ma ZH, Li Q, Yue QY, Gao BY, Li WH, Xu X, Zhong QQ (2011) Adsorption removal of ammonium and phosphate from water by fertilizer controlled release agent prepared from wheat straw. *Chem Eng J* 171(3):1209–1217. <https://doi.org/10.1016/j.cej.2011.05.027>
- Mašek O, Brownsort P, Cross A, Sohi S (2013) Influence of production conditions on the yield and environmental stability of biochar. *Fuel* 103:151–155. <https://doi.org/10.1016/j.fuel.2011.08.044>
- Özcar M (2003) Equilibrium and kinetic modelling of adsorption of phosphorus on calcined alunite. *Adsorption J Int Adsorpt Soc* 9(2):125–132. <https://doi.org/10.1023/A:1024289209583>
- Paerl HW (2009) Controlling eutrophication along the freshwater–marine continuum: dual nutrient (N and P) reductions are essential. *Estuar Coasts* 32(4):593–601. <https://doi.org/10.1007/s12237-009-9158-8>
- Pan J, Jiang J, Xu R (2013) Adsorption of Cr(III) from acidic solutions by crop straw derived biochars. *J Environ Sci* 25(10):1957–1965. [https://doi.org/10.1016/S1001-0742\(12\)60305-2](https://doi.org/10.1016/S1001-0742(12)60305-2)
- Park JH, Ok YS, Kim SH, Cho JS, Heo JS, Delaune RD, Seo DC (2015) Evaluation of phosphorus adsorption capacity of sesame straw biochar on aqueous solution: influence of activation methods and pyrolysis temperatures. *Environ Geochem Health* 37(6):969–983. <https://doi.org/10.1007/s10653-015-9709-9>
- Radnia H, Ghoreyshi AA, Younesi H (2011) Isotherm and kinetics of Fe(II) adsorption onto chitosan in a batch process. *Iran J Energy Environ* 2:250–257
- Ren J, Li N, Li L, An JK, Zhao L, Ren NQ (2015) Granulation and ferric oxides loading enable biochar derived from cotton stalk to remove phosphate from water. *Bioresour Technol* 178:119–125. <https://doi.org/10.1016/j.biortech.2014.09.071>
- Sarkhot DV, Ghezzehei TA, Berhe AA (2013) Effectiveness of biochar for sorption of ammonium and phosphate from dairy effluent. *J Environ Qual* 42(5):1545–1554. <https://doi.org/10.2134/jeq2012.0482>
- Sellaoui L, Dotto GL, Lamine AB, Erto A (2017a) Interpretation of single and competitive adsorption of cadmium and zinc on activated carbon using monolayer and exclusive extended monolayer models. *Environ Sci Pollut Res* 24(24):19902–19908. <https://doi.org/10.1007/s11356-017-9562-8>
- Sellaoui L, Franco DSP, Dotto GL, Lima ÉC, Lamine AB (2017b) Single and binary adsorption of cobalt and methylene blue on modified chitin: application of the hill and exclusive extended hill models. *J Mol Liq* 233:543–550. <https://doi.org/10.1016/j.molliq.2016.10.079>
- Smith VH (2003) Eutrophication of freshwater and coastal marine ecosystems a global problem. *Environ Sci Pollut Res* 10(2):126–139. <https://doi.org/10.1065/espr2002.12.142>
- Tseng RL, Wu FC (2008) Inferring the favorable adsorption level and the concurrent multi-stage process with the Freundlich constant. *J Hazard Mater* 155(1-2):277–287. <https://doi.org/10.1016/j.jhazmat.2007.11.061>
- Verheijen FGA, Jeffery S, Bastos AC, van der Velde M, Diafas I (2009) Biochar application to soils—a critical scientific review of effects on soil properties, processes and functions. EUR 24099 EN. Office for Official Publications of the European Communities, Luxembourg
- Wahab M, Jellali S, Jedidi N (2010) Ammonium biosorption onto sawdust: FTIR analysis, kinetics and adsorption isotherms modeling. *Bioresour Technol* 101(14):5070–5075. <https://doi.org/10.1016/j.biortech.2010.01.121>
- Wang H, Gao B, Wang S, Fang J, Xue Y, Yang K (2015a) Removal of Pb(II), Cu(II), and Cd(II) from aqueous solutions by biochar derived from KMnO₄ treated hickory wood. *Bioresour Technol* 197:356–362. <https://doi.org/10.1016/j.biortech.2015.08.132>

- Wang ZH et al (2015b) Biochar produced from oak sawdust by Lanthanum (La)-involved pyrolysis for adsorption of ammonium (NH_4^+), nitrate (NO_3^-), and phosphate (PO_4^{3-}). *Chemosphere* 119: 646–653. <https://doi.org/10.1016/j.chemosphere.2014.07.084>
- Yao Y, Gao B, Chen JJ, Yang LY (2013) Engineered biochar reclaiming phosphate from aqueous solutions: mechanisms and potential application as a slow-release fertilizer. *Environ Sci Technol* 47(15):8700–8708. <https://doi.org/10.1021/es4012977>
- Yao Y, Gao B, Inyang M, Zimmerman AR, Cao XD, Pullammanappallil P, Yang LY (2011a) Biochar derived from anaerobically digested sugar beet tailings: characterization and phosphate removal potential. *Bioresour Technol* 102(10):6273–6278. <https://doi.org/10.1016/j.biortech.2011.03.006>
- Yao Y, Gao B, Inyang M, Zimmerman AR, Cao XD, Pullammanappallil P, Yang LY (2011b) Removal of phosphate from aqueous solution by biochar derived from anaerobically digested sugar beet tailings. *J Hazard Mater* 190(1-3):501–507. <https://doi.org/10.1016/j.jhazmat.2011.03.083>
- Yu JT, Dehkhoda AM, Ellis N (2010) Development of biochar-based catalyst for transesterification of canola oil. *Energy Fuel* 25:337–344
- Zhang M, Gao B, Yao Y, Xue YW, Inyang M (2012) Synthesis of porous MgO-biochar nanocomposites for removal of phosphate and nitrate from aqueous solutions. *Chem Eng J* 210:26–32. <https://doi.org/10.1016/j.ccej.2012.08.052>
- Zhang T, Li Q, Ding L, Ren H, Xu K, Wu Y, Sheng D (2011) Modeling assessment for ammonium nitrogen recovery from wastewater by chemical precipitation. *J Environ Sci* 23(6):881–890. [https://doi.org/10.1016/S1001-0742\(10\)60485-8](https://doi.org/10.1016/S1001-0742(10)60485-8)
- Zhang Y, Li ZF, Mahmood IB (2014) Recovery of NH_4^+ by corn produced biochars and its potential application as soil conditioner. *Front Environ Sci Eng China* 8:825–834
- Zhao L, Cao X, Mašek O, Zimmerman A (2013) Heterogeneity of biochar properties as a function of feedstock sources and production temperatures. *J Hazard Mater* 256–257:1–9. <https://doi.org/10.1016/j.jhazmat.2013.04.015>
- Zheng W, Guo MX, Chow T, Bennett DN, Rajagopalan N (2010) Sorption properties of green waste biochar for two triazine pesticides. *J Hazard Mater* 181(1-3):121–126. <https://doi.org/10.1016/j.jhazmat.2010.04.103>